

Optimal point for solid state two-qubit gates in a fixed coupling scheme

E. Paladino,¹ A. Mastellone,^{2,1} A. D'Arrigo,¹ and G. Falci¹

¹*Dipartimento di Metodologie Fisiche e Chimiche (DMFCI),
Università di Catania. Viale A. Doria 6, 95125 Catania (Italy) & MATIS CNR - INFN, Catania*
²*C.I.R.A. Centro Italiano Ricerche Aerospaziali - Via Maiorise snc - 81043 Capua, CE (Italy)*

We present a route to single out two-qubit optimal points within fixed coupling schemes. We demonstrate that, for selected *optimal couplings*, a high-efficiency universal two-qubit gate can be implemented even in the presence of the detrimental $1/f$ noise sources. Entanglement generation and degradation due to interplay of $1/f$ and quantum noise is quantified via the concurrence. This characterization directly translates to measurable quantities. The possibility to implement a faithful superconducting i -SWAP gate for spectra extrapolated from single qubit experiments is pointed out.

PACS numbers: 03.65.Yz, 03.67.Lx, 05.40.-a

Keywords: decoherence; $1/f$ -noise; quantum control.

The implementation of a universal two-qubit gate involving an entanglement operation on two quantum bits represents a necessary step toward the construction of a scalable quantum computer [1]. Intense research on solid state nanodevices during the last decade has established potentiality to combine quantum coherent behavior with the existing integrated-circuit fabrication technology. We mention, e. g., the variety of high-fidelity single qubit gates based on superconducting technologies nowadays available [2, 3]. However the best way to achieve controllable coupling and a universal two-qubit gate are still open questions. A number of theoretical proposals [4, 5, 6, 7] and experimental attempts have been put forward [8, 9].

The most natural way to realize two-qubit entanglement is via a fixed, capacitive or inductive, coupling scheme [4]. With tunable single-qubit energy spacing, fixed coupling has been used to demonstrate two-qubit logic gates [8]. In order to achieve mutual resonance during the gate operation at least one qubit has to be moved away from the working point of minimal sensitivity to parameters variations, the "optimal point" [2, 3]. This is so far the main drawback of fixed-coupling schemes for most of the Josephson implementations. Recent proposals have attempted to solve this problem by tunable coupling schemes [5, 6]. Most of them rely on additional circuit elements, such as switchable Josephson junctions, inductors, lumped or cavity-type resonators or further qubits. Some of them gain their tunability from ac-driving [6], others from "adiabatic" couplers [7]. Some of these schemes have been experimentally tested and are potentially scalable [9]. However, none of these implementations is totally immune from imperfections. Some ac-schemes require strong driving or result in slow operations and non-adiabatic corrections may prevent complete switching-off of adiabatic couplers [10]. Cross-talk due to always-on coupling and to measurement is present also in most of the ac-driven operational modes. Moreover, any additional circuit element is a new port to noise.

In this scenario it is therefore relevant to critically re-

view the possibility to employ "minimal" fixed coupling schemes. In non-tunable NMR coupling strategies a fraction of quantum operations is devoted to effective decoupling procedures, possibly resulting in difficult scalability. In this Letter we will instead introduce a strategy to single out *two-qubit optimal points* within fixed coupling schemes. Fast two-qubit operations and switching on/off the coupling can be achieved by individual-qubit control. Very small fluctuations are introduced by the minimal additional circuitry. We consider independent noise sources acting on individual qubits along both transverse and longitudinal directions [11]. We demonstrate that, for selected *optimal couplings*, an efficient universal two-qubit gate can be implemented even in the presence of the detrimental $1/f$ noise sources. We first investigate a nanodevice model system and find analytic results for the coupled dynamics. We specify to a imaginary-SWAP (i -SWAP) gate implemented by capacitively coupled charge-phase qubits [3] and suggest that for experimental spectra a sufficiently faithful gate is within reach with present technology. The analysis is supported by numerical solution of the stochastic Schrödinger equation in the 4-dim Hilbert space in the presence of bistable fluctuations leading to $1/f$ [12] and white noise.

Model and optimal coupling – In fixed coupling schemes the interaction is effectively switched on by tuning the single-qubit energy spacing to mutual resonance. The building-block Hamiltonian reads $\mathcal{H}_0 = -\frac{\Omega}{2} \sigma_3^{(1)} \otimes \mathbb{1}^{(2)} - \frac{\Omega}{2} \mathbb{1}^{(1)} \otimes \sigma_3^{(2)} + \frac{\omega_c}{2} \sigma_1^{(1)} \otimes \sigma_1^{(2)}$ ($\hbar = 1$, $\sigma_3^{(\alpha)} |\pm\rangle = \pm |\pm\rangle$). The Hilbert space factorizes in a "SWAP-subspace", spanned by the eigenstates of \mathcal{H}_0 $\{|1\rangle = \frac{1}{\sqrt{2}} (|-+\rangle + |+-\rangle)$ and $|2\rangle = \frac{1}{\sqrt{2}} (|+-\rangle + |-+\rangle)\}$ (eigenvalues $\omega_{\frac{1}{2}} = \mp\omega_c/2$), and in a "Z-subspace" generated by the eigenstates $\{|0\rangle = -\sin\frac{\varphi}{2} |++\rangle + \cos\frac{\varphi}{2} |--\rangle$ and $|3\rangle = \cos\frac{\varphi}{2} |++\rangle + \sin\frac{\varphi}{2} |--\rangle\}$, where $\tan\varphi = -\omega_c/(2\Omega)$ (eigenvalues $\omega_0 = \mp\sqrt{\Omega^2 + (\omega_c/2)^2}$). We focus on the i -SWAP operation $|+-\rangle \rightarrow |\psi_e\rangle = [|+-\rangle - i| -+\rangle]/\sqrt{2}$ which generates an entangled state by free evolution for a time $t_E = \pi/2\omega_c$.

The gate efficiency is limited by fluctuations of the con-

control parameters due to external environments. We model them by adding to \mathcal{H}_0 , $\mathcal{H}_I = -\frac{1}{2} [\hat{x}_1\sigma_1^{(1)} + \hat{y}_1\sigma_3^{(1)}] \otimes \mathbb{1}_2 - \frac{1}{2} \mathbb{1}_1 \otimes [\hat{x}_2\sigma_1^{(2)} + \hat{y}_2\sigma_3^{(2)}]$. Here \hat{x}_i, \hat{y}_i are collective environmental variables. Since in relevant situations transverse (\hat{x}_i) and longitudinal (\hat{y}_i) fluctuations have different physical origin, we assume they are independent. Typically the corresponding power spectra display a $1/f$ low-frequency behavior up to some cut-off frequency followed by a white or ohmic flank [14, 15]. Low-frequency fluctuations can be approximated as classical stochastic processes $\hat{x}_i \rightarrow x_i(t)$, $\hat{y}_i \rightarrow y_i(t)$ [13]. Their leading effect is to randomize clock frequencies, therefore the average of several measurements is defocused, analogously to inhomogeneous broadening. Partial reduction of this effect may be achieved by operating the device at optimal points, characterized by minimal sensitivity of the relevant splittings to variations of the control parameters. In single qubit two-port architectures [14] a “sweet spot” is found at a saddle point of the energy bands, where both transverse and longitudinal noises are partly decoupled.

In the two-qubit setup the relevant scale for the i -SWAP gate is the “effective” splitting in the SWAP subspace, $\omega_{21}(x_1, y_1, x_2, y_2)$ obtained from $\mathcal{H}_0 + \mathcal{H}_I$ treating perturbatively the stochastic fields in \mathcal{H}_I ,

$$\begin{aligned} \omega_{21}(x_1, x_2, y_1, y_2) &\approx \omega_c - \frac{\omega_c}{2\Omega^2}(x_1^2 + x_2^2) + \frac{1}{2\omega_c}(y_1 - y_2)^2 \\ &+ \frac{\omega_c}{2\Omega^3}(x_1^2 + x_2^2)(y_1 + y_2) + \frac{1}{2\omega_c\Omega}(x_1^2 - x_2^2)(y_1 - y_2) \quad (1) \\ &+ \frac{\omega_c}{8\Omega^4}\left(1 + \frac{\omega_c^2}{\Omega^2}\right)(x_1^4 + 6x_1^2x_2^2 + x_2^4) + \frac{1}{8\omega_c\Omega^2}(x_1^2 - x_2^2)^2. \end{aligned}$$

A key feature is that ω_{21} is non-monotonic in ω_c , i. e. second order transverse corrections are $\propto \omega_c$, whereas longitudinal ones vary as ω_c^{-1} . The different behavior is due to a selection rule for longitudinal fluctuations. They only mix states inside each - SWAP or Z - subspace, while x_i -fluctuations mix the two subspaces. Non-monotonic behavior in the small coupling energy $\omega_c \ll \Omega$ is crucial for the identification of the optimal working point. Indeed an *optimal coupling* can be found when the variance of the stochastic splitting $\delta\omega_{21} = \omega_{21}(x_1, x_2, y_1, y_2) - \omega_c$, $\Sigma_{21}^2 = \langle \delta\omega_{21}^2 \rangle$, is minimal. Here we have

$$\Sigma_{21}^2 \approx \frac{1}{\omega_c^2} \left\{ \left(\frac{\Sigma_x}{\Omega} \right)^4 [(\Sigma_x^2 - \omega_c^2)^2 + \Sigma_x^4 + \Sigma_{y_2}^2 \Omega^2] + \frac{\Sigma_{y_2}^4}{2} \right\} \quad (2)$$

where we took Gaussian distributed x_i and y_i and assumed equal transverse variances, $\Sigma_{x_i} = \Sigma_x$ and $\Sigma_{y_1} \ll \Sigma_{y_2}$, which mimic typical experimental conditions. Eqs. (1) - (2) are the first important result of this Letter: while higher stability with respect to *longitudinal* fluctuations is attained by larger couplings, minimization of the detrimental *transverse* low-frequency noise components is obtained by tuning the coupling to an *optimal value*

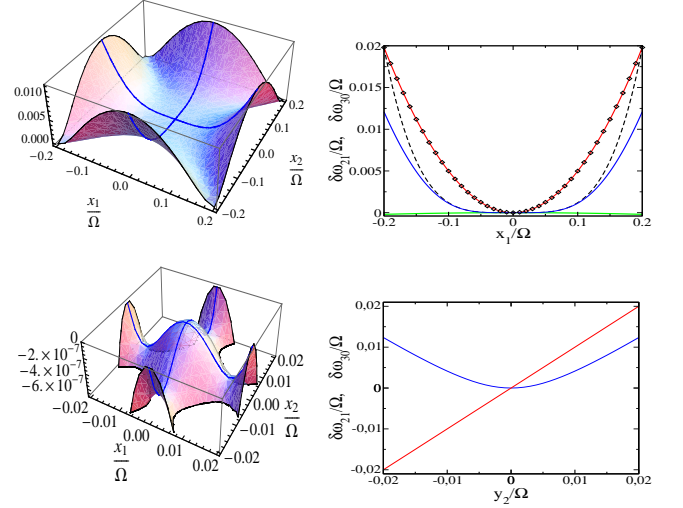


FIG. 1: Dispersion of the SWAP and Z splittings for $\omega_c/\Omega = 0.01$. Left: $\delta\omega_{21}/\Omega$ from numerical diagonalization of $\mathcal{H}_0 + \mathcal{H}_I$ (top). Zoom around the origin highlights the interplay of 2^{nd} and 4^{th} order terms, barrier height $\propto \omega_c^3$ (bottom). Right: Comparative behavior of dispersions in the two subspaces. Top: SWAP exact splitting (blue), expansion (1) for $x_2 = 0$, $y_i = 0$ (black dashed), 2^{nd} order expansion (green), Z splitting (red) $\delta\omega_{30} \simeq -\frac{\cos\varphi}{2} \left\{ (y_1 + y_2) + \left[1 + \frac{1}{2} \left(\frac{\omega_c}{\Omega} \right)^2 \right] \frac{x_1^2 + x_2^2}{\Omega} \right\}$, and single qubit dispersion (diamonds). Bottom: Longitudinal dispersions. The Z-subspace (red lines) is much more sensitive both to transverse and longitudinal variations.

$\tilde{\omega}_c$. For $\Sigma_{y_2} \ll \Sigma_x$, this is the transverse noise variance, $\tilde{\omega}_c \approx 2^{1/4} \Sigma_x$. It can be estimated by independent measurement of the amplitude of the $1/f$ transverse noise on the uncoupled qubits, $S_x^{1/f} = \pi \Sigma_x^2 [\ln(\gamma_M/\gamma_m) \omega]^{-1}$, $\Sigma_x^2 = \int_0^\infty d\omega/\pi S_x^{1/f}(\omega)$ (low and high frequency cut-offs γ_m and γ_M). Non-monotonicity in ω_c results in a (not intuitive) competition between 2^{nd} and 4^{th} order x_i -terms in Eq.(1), Figure 1 (left). As a result of this at first sight tiny feature, identification of the best operating condition necessarily requires consideration of the noise characteristics. Note the higher stability of the SWAP-splitting compared both to the uncoupled qubits Larmor frequency and the Z-splitting, Figure 1 (right).

i-SWAP gate – Working at the optimal coupling minimizes defocusing and guarantees excellent performance of the *i*-SWAP operation. As a unambiguous test of entanglement generation and its degradation due to noise, we calculated the concurrence during the gate operation [16]. Upon extending the multi-stage elimination approach [13], we first separate the effects of low- and high-frequency components of the noise by putting, e. g., $\hat{x}_i \rightarrow x_i(t) + \hat{x}_i^f$. Stochastic variables $x_i(t)$ describe low-frequency ($1/f$) noise, and can be treated in the adiabatic and longitudinal approximation. High-frequency ($\omega \geq \omega_c$) fluctuations \hat{x}_i^f are modeled by a Markovian bath and mainly determine spontaneous decay. There-

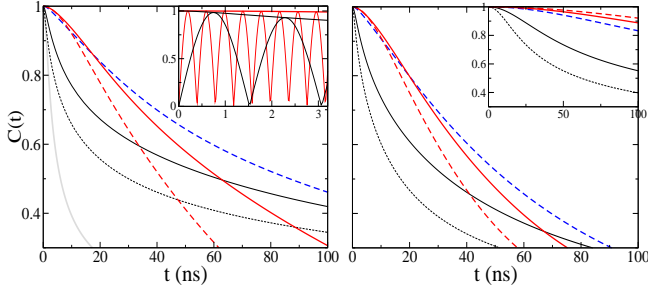


FIG. 2: Envelope of the concurrence in the SPA, $\Omega = 10^{11}$ rad/s. Left: Effect of transverse noise with $\Sigma_x/\Omega = 0.08$ and $\omega_c/\Omega = 0.01, 0.02, 0.06, 0.08, 0.1$ (black-dashed, black, blue, red, red-dashed). Gray is the single qubit coherence, $|\rho_{+-}(t)| = [1 + (\Sigma_x^2 t/\Omega^2)]^{-1/4}$ [13]. Inset: $C(t)$ and its envelope for $\omega_c/\Omega = 0.02, 0.08$. For optimal coupling $\tilde{\omega}_c \approx \Sigma_x$, at 3ns already 8-SWAP cycles occurred. Right: Effect of transverse plus longitudinal noise on qubit 2, $\Sigma_{y2}/\Omega = 2.5 \times 10^{-3}$. Inset: Effect of longitudinal noise, ω_c values as in left panel.

fore, populations relax due to quantum noise (T_1 -type times), which also leads to secular dephasing ($T_2^* = 2T_1$ -type). Low-frequency noise provides a defocusing mechanism determining further decay of the coherences.

The system is initialized in $|+-\rangle$ by applying a π -pulse on qubit 2 starting from uncoupled ground state $|++\rangle$. Starting inside the SWAP subspace, the 4×4 density matrix in the computational basis is non-vanishing only along the diagonal and anti-diagonal at any time. For such “X-states” the concurrence takes a simple form [17].

We first consider the effect of low-frequency fluctuations, and indicate with $\mathbf{z}(t) = \{z_i\} = \{x_1, x_2, y_1, y_2\}$ an individual realization of the stochastic process. In the adiabatic approximation, the concurrence simplifies to $C(t) = 2 |\text{Im}\{\rho_{12}(t)\}|$, where $\rho_{ij}(t)$ are entries of the two-qubit density matrix in the eigenbasis. The leading effect of low-frequency fluctuations in repeated measurements protocols is given within the Static Path Approximation, by $\rho_{ij}(t) \approx \rho_{ij}(0) \int d\mathbf{z} P(\mathbf{z}) \exp[-i\omega_{ij}(\mathbf{z})t]$ [13]. The probability density can be assumed of Gaussian form $P[z_i] = \exp[-z_i^2/2\Sigma_{z_i}^2]/\sqrt{2\pi\Sigma_{z_i}}$. With the SWAP-splitting expansion (1) (including in the 3rd and 4th order the terms $\propto \omega_c^{-1}$) we obtain

$$\rho_{12}(t) = \rho_{12}(0) \frac{\Omega}{2\Sigma_x^2} \sqrt{\frac{2i\omega_c}{\pi t}} e^{i\omega_c t + h(t)} K_0[h(t)] \quad (3)$$

where $h(t) = (\Sigma_{y1}^2 + \Sigma_{y2}^2 + i\omega_c/t) (\Omega^2/\Sigma_x^2 + i\omega_c t)^2 / (4\Omega^2)$, and $K_0[h]$ is the K-Bessel function of order zero [18]. By increasing the coupling to match the optimal condition two goals are simultaneously achieved: minimization of initial defocusing and fast two-qubit gate (Figure 2). The first SWAP error takes remarkable values $\varepsilon = 1 - \langle \psi_e | \rho(t_E) | \psi_e \rangle \approx 10^{-3} - 10^{-4}$, for $\omega_c \approx \Sigma_x \leq 0.05\Omega$ (numerical simulations). For such a large $1/f$ noise amplitude single qubit coherence times would be rather small $T_2 \approx 5$ ns ($T_2 \approx 30$ ns from transverse $1/f$ noise).

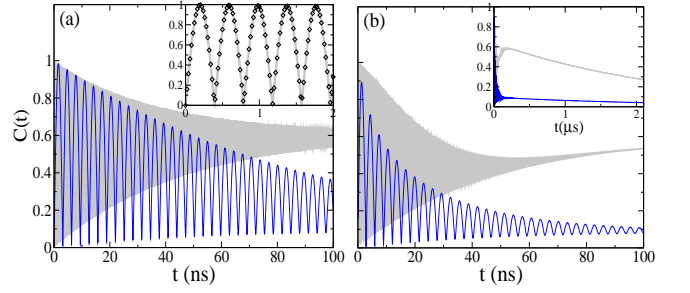


FIG. 3: Concurrence for $\omega_c/\Omega = 0.01$ (blue) and optimal coupling $\tilde{\omega}_c/\Omega = 0.08$ (gray). (a) Effect of high-frequency noise, $S_{x_i}(\omega) \approx 8 \times 10^5 \text{s}^{-1}$, $S_{y_2}(\omega) \approx 4 \times 10^7 \text{s}^{-1}$. Inset: At short times $C(t) \approx 2|\text{Im}\{\rho_{12}(t)\}|$ (diamonds). (b) Effect of $1/f$ noise (parameters as in Fig. 2) and white quantum noise. Inset: Asymptotic behavior. Results are minimally modified considering the dynamics of fluctuators generating $1/f$ transverse (longitudinal) noise in $\gamma_m = 1 \text{s}^{-1}$, $\gamma_M = 10^6$ (10^{10}) s^{-1} (numerical solution of the stochastic Schrödinger equation).

Within the secular approximation, high-frequency noise leads to additional exponential decay of SWAP-coherence, $\tilde{\rho}_{12}(t) = \rho_{12}(t) \exp\{-\tilde{\Gamma}_{12}t\}$. The SWAP decay rate $\tilde{\Gamma}_{12}$ results from inelastic processes between subspaces and inside the SWAP subspace. Since $k_B T \ll \Omega$, thermal excitation processes between subspaces can be neglected and $\tilde{\Gamma}_{12} \approx (\Gamma_1^e + \Gamma_2^e)/2$. The escape rates from levels 1 and 2, $\Gamma_1^e = \Gamma_{10} + \Gamma_{12}$, $\Gamma_2^e = \Gamma_{20} + \Gamma_{21}$ depend on the noise spectra $S_{z_i}(\omega)$,

$$\begin{aligned} \Gamma_{10} &= \frac{1}{4} (1 + \sin \varphi) [S_{x_1}(\omega_{10}) + S_{x_2}(\omega_{10})] \\ \Gamma_{20} &= \frac{1}{4} (1 - \sin \varphi) [S_{x_1}(\omega_{20}) + S_{x_2}(\omega_{20})] \\ \Gamma_{21} &= \frac{1}{2} [S_{y_1}(\omega_{21}) + S_{y_2}(\omega_{21})]. \end{aligned} \quad (4)$$

These rates enter the populations $\rho_{ii}(t)$, $i = 0, 1, 2$ in the combinations $\Gamma_{\pm} = -(\Gamma_1^e + \Gamma_2^e)/2 \pm \sqrt{(\Gamma_1^e - \Gamma_2^e)^2 + 4\Gamma_{12}\Gamma_{21}}/2$ [19]. Under these conditions $\rho_{33}(t) \equiv 0$ and the concurrence reads $C(t) \approx \sqrt{(\rho_{11} - \rho_{22})^2 + 2(\text{Im}\{\tilde{\rho}_{12}\})^2} - |\sin \varphi| \rho_{00}$. The optimal coupling scheme is effective against large amplitude $1/f$ noise even in the presence of high-frequency fluctuations, Figure 3. The SWAP-coherence rules the relevant short-time behavior, $|\rho_{12}| \propto 1 - \tilde{\Gamma}_{12}t$ (or $|\rho_{12}| \propto 1 - (\Sigma_{21}t)^2/2$) depending on the most relevant quantum (or adiabatic) noise component. At longer times decay turns to exponential. If longitudinal noise prevails, $C(t) \approx |\rho_{11}(t) - \rho_{22}(t)| \approx \tanh(\frac{\omega_c}{2k_B T}) \{1 - e^{-(S_{y_2} + S_{y_1})t/2}\}$, while if transverse noise dominates, $C(t) \approx |\sin \varphi| \rho_{00}(t) \approx |\sin \varphi| \{1 - [e^{-\Gamma_{10}t} + e^{-\Gamma_{20}t}]/2\}$. The finite asymptotic value reflects entanglement of the thermalized state (no “entanglement sudden death” occurs [17]).

Charge-phase i-SWAP gate – The above entanglement characterization translates into directly measurable quantities. Here we specialize to charge-phase qubits [3, 14] and to independent measurements (bitwise readout). Individual qubit control is achieved via gate voltages V_g and magnetic-flux dependent phases δ_i , enter-

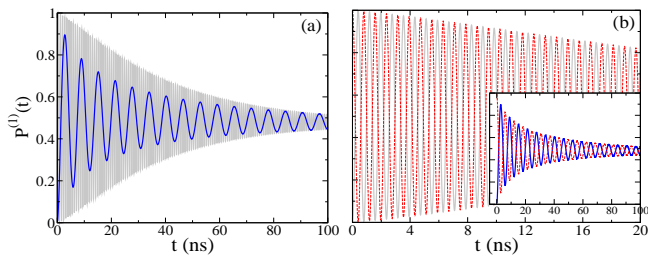


FIG. 4: Switching probabilities in the presence of $1/f$ and white noise, $\omega_c/\Omega = 0.01$ (blue) and optimal coupling $\tilde{\omega}_c = \Sigma_x = 0.08\Omega$ (gray). (a) $P^{(1)}(t)$: Exponential short-time limit at $\tilde{\omega}_c$, algebraic otherwise. (b) $P^{(1)}(t)$ and $P^{(2)}(t)$ (red) anti-phase oscillations for $\tilde{\omega}_c$ (main), $\omega_c/\Omega = 0.01$ (inset).

ing the Josephson energy $E_{J,i} = E_{J,i}^0 \cos \delta_i$. The optimal point for the uncoupled qubits is $q_{x,i} \equiv C_g V_g / (2e) = 1/2$, $\delta_i = 0$ [3]. Polarization fluctuations cause transverse noise $x_i \propto 4E_{C,i} \Delta q_{i,x}$ ($E_{C,i}$ qubit i charging energy), phase fluctuations lead to longitudinal noise $y_i \propto \Delta E_{J,i}$. Resonance/detuning is achieved by keeping $q_{i,x} = 1/2$, $\delta_1 = 0$ and tuning δ_2 . For set of parameters close to those planned in experiments [20] resonance occurs for $\delta_2 \approx 0.45$, and model \mathcal{H}_0 applies. We considered noise figures extrapolated from single-qubit data reported in Refs [3, 14]. Since both qubits operate at $q_{i,x} = 1/2$ we expect similar polarization fluctuations. To elucidate the significance of the optimal coupling scheme, we intentionally considered $1/f$ noise amplitudes larger than expected from single qubit measurements, $\Sigma_x \approx 0.02\Omega$, $\Sigma_{y_2} \approx 8 \times 10^{-4}\Omega$ [13, 14]. Phase noise on qubit 1 operating at the sweet spot is negligible [22].

Initializing $|+\rangle$, bitwise readout gives the qubit 1 switching probability to state $|-\rangle$, $P^{(1)}(t)$ and the probability $P^{(2)}(t)$ to find qubit 2 in the initial state $|-\rangle$. Out of phase oscillations signals two-qubit states anti-correlations and follows from $P^{(2)}(t) = P(t) \pm \text{Re}[\rho_{12}(t)]$, with $P(t) = -\frac{1}{2} \cos \varphi [\rho_{11}(t) + \rho_{22}(t)] + \cos^2(\frac{\varphi}{2})$. For optimal coupling, defocusing due to $1/f$ polarization and phase noise is considerably reduced and phase quantum noise on the qubit displaced by its optimal point $\delta_2 \neq 0$ contributes to initial decay, Figure 4. Note that oscillations visibility larger than 90% persists until ≈ 10 ns, corresponding to about 25 SWAP cycles. This contrasts with strong initial suppression of oscillations for non-optimal coupling. The long time exponential behavior is dominated by polarization quantum noise.

According to the present analysis, fixed-optimal-coupling two-qubit gates based on charge-phase qubits should be within reach with present technology, even in the presence of large amplitude $1/f$ polarization fluctuations. The recipe requires preliminary noise characterization and work in the protected SWAP-subspace. The device reliability may however be qualified by the impact of one/few impurities strongly coupled to one or both

qubits [13, 21]. These may induce non-Gaussian fluctuations which randomly displace qubits from resonant condition, possibly resulting in limited readout fidelity [20]. These effects are beyond the present analysis. They still represent a limiting factor for solid-state nanodevices.

We acknowledge discussions with D. Vion, U. Weiss, A. G. Mauger and support from EU-EuroSQIP (IST-3-015708-IP).

-
- [1] M. Nielsen, I. Chuang, "Quantum Computation and Quantum Information", Cambridge Univ. Press, 2005.
 - [2] Y. Nakamura *et al.*, Nature **398**, 786 (1999); Y. Yu *et al.*, Science **296**, 889 (2002); J.M. Martinis *et al.*, Phys. Rev. Lett. **89**, 117901 (2002); I. Chiorescu *et al.*, Science, **299**, 1869, (2003); T. Yamamoto *et al.*, Nature **425**, 941 (2003); S. Saito *et al.*, Phys. Rev. Lett. **93**, 037001 (2004); J. Johansson *et al.*, *ibid.* **96**, 127006 (2006); F. Deppe *et al.*, Nat. Phys. **4**, 686 (2008); J. A. Schreier *et al.*, Phys. Rev. B **77**, 180502(R) (2008).
 - [3] D. Vion *et al.*, Science **296**, 886 (2002).
 - [4] Yu. Makhlin *et al.*, Nature **398**, 305 (1999); J. Q. You *et al.*, Phys. Rev. Lett. **89**, 197902 (2002).
 - [5] D.V. Averin, C. Bruder, Phys. Rev. Lett. **91**, 057003 (2003); A. Blais *et al.*, *ibid.* **90**, 127901 (2003); F. Plastina, G. Falci, Phys. Rev. B **67**, 224514 (2003); B. Plourde *et al.*, *ibid.* **70**, 140501(R) (2004); A.O. Niskanen, Y. Nakamura, J.S. Tsai, *ibid.* **73**, 094506 (2006); P. Bertet, C. J. Harmans, J.E. Mooij, *ibid.* **73**, 064512 (2006); Y-D Wang, A. Kemp, K. Semba, *ibid.* **79**, 024502 (2009).
 - [6] C. Rigetti, A. Blais, and M. Devoret, Phys. Rev. Lett. **94**, 240502 (2005); Yu-xi Liu *et al.*, *ibid.* **96**, 067003 (2006); G. S. Paraoanu, Phys. Rev. B **74**, 140504(R) (2006).
 - [7] T. V. Filippov *et al.*, IEEE Trans. Appl. Supercond. **13**, 1005 (2003); A. Maassen van den Brink *et al.*, New J. Phys. **7**, 230 (2005).
 - [8] Yu. A. Pashkin *et al.*, Nature **421**, 823 (2003); A. J. Berkley *et al.*, Science **300**, 1548 (2003); T. Yamamoto *et al.*, Nature **425**, 941 (2003); J. B. Majer *et al.*, Phys. Rev. Lett. **94**, 090501 (2005); J.H. Plantenberg *et al.*, Nature **447**, 836 (2007).
 - [9] A. Izmalkov *et al.*, Phys. Rev. Lett. **93**, 037003 (2004); T. Hime *et al.*, Science **314**, 1427 (2006); A. O. Niskanen *et al.*, Science **316**, 723 (2007); A. O. Niskanen *et al.*, Nature **447**, 386 (2007); J. Majer *et al.*, *ibid.* **449**, 443 (2007); S. H. W. van der Ploeg *et al.*, Phys. Rev. Lett. **98**, 057004 (2007); A. Fay *et al.*, *ibid.* **100**, 187003 (2008).
 - [10] C. Hutter *et al.*, Europhys. Lett. **74**, 1088 (2006).
 - [11] Correlated noise and cross-talk effects have been addressed in A. D'Arrigo *et al.* NJP **10**, 115006 (2008).
 - [12] E. Paladino *et al.*, Phys. Rev. Lett. **88**, 228304 (2002).
 - [13] G. Falci *et al.*, Phys. Rev. Lett. **94**, 167002 (2005).
 - [14] G. Ithier *et al.*, Phys. Rev. B **72**, 134519 (2005).
 - [15] O. Astafiev *et al.*, Phys. Rev. Lett. **93**, 267007 (2004).
 - [16] W. K. Wothers Phys. Rev. Lett. **80**, 2245 (1998).
 - [17] T. Yu, J. H. Eberly, Phys. Rev. Lett. **97**, 140403 (2006).
 - [18] M. Abramowitz, I. A. Stegun "Handbook of Mathematical Functions", Dover (1965).
 - [19] E. Paladino *et al.* Physica E in press (2009).
 - [20] D. Vion, private communication. $E_C \simeq 10$ GHz, $E_J \simeq$

14 GHz implying $\Omega \approx 8 \times 10^{10}$ rad/s, $\omega_c \approx 1.2 \times 10^9$ rad/s.

- [21] Y. M. Galperin *et al.* Phys. Rev. Lett. **96**, 097009 (2006).
 [22] From Ref. [14] $\Sigma_{y_1}/\Omega \approx 10^{-5}$ and $S_{\delta_1}(\omega) \approx 3.7 \times 10^{-14}$ s at $\omega \geq 10^7 \text{ s}^{-1}$, implying $S_{y_1}(\omega) =$

$$2S^2/(\pi\Omega^2)\omega \coth(\omega/(2K_B T)), \text{ with } S = 9 \times 10^7 \text{ s}^{-1};$$

$$S_{y_1}(\omega_c = 0.08\Omega) \approx 6 \times 10^3 \text{ s}^{-1} \text{ [19].}$$